

Evidence for a very-long-term trend in geomagnetic secular variation

ANDREW J. BIGGIN*, GEERT H. M. A. STRIK AND COR G. LANGEREIS

Palaeomagnetic Laboratory Fort Hoofddijk, Budapestlaan 17, Universiteit Utrecht, Utrecht 3584 CD, Netherlands

*e-mail: biggin@geo.uu.nl

Published online: 4 May 2008; doi:10.1038/ngeo181

The Earth's inner core is believed to inhibit rapid fluctuations in the geomagnetic field from developing into full polarity reversals^{1,2}. Consequently, during the Precambrian, the smaller size of the inner core might suggest that polarity reversals could occur more readily. It is therefore surprising that there are indications that reversals were rare during this period^{3,4}. Here we use new and existing palaeomagnetic data from three continents to examine the stability of the Earth's magnetic field from 2.82 to 2.45 billion years ago. We show that, on average, geomagnetic secular variation (the field variations produced by normal geodynamo action) during the late Archaean and early Proterozoic was different from that of the past 200 million years; specifically, the apparent variability of the geomagnetic pole as viewed at low and mid-latitudes was reduced relative to the past 200 million years. According to both dynamo simulations⁴ and more recent palaeomagnetic field observations⁵, the observed pattern of secular variation suggests a lower frequency of polarity reversals 2.5 billion years ago. This may imply that the geodynamo is becoming progressively less stable over long timescales, consistent with some numerical simulations^{6,7}, possibly as a result of changing outer-core geometry that has accompanied inner-core growth.

Our confidence in claims^{3,4} that the geomagnetic field reversed its polarity less frequently in the Precambrian period (>542 Myr) than in the Phanerozoic is limited by the lack of long continuous Precambrian magnetostratigraphic sections. Fortunately, analyses of geomagnetic palaeosecular variation (PSV)—the record of ancient secular variation—provide an independent means of assessing the stability of the geomagnetic field and have the added advantage that they do not require rocks to form continuous time series as do magnetostratigraphic studies.

A recent study analysed PSV (ref. 8) in the late Archaean to earliest Proterozoic and concluded that it was similar to that of the past 5 Myr. The present study focuses on approximately the same time period (about 2.45–2.82 Gyr), as it is the oldest for which there is a sufficient (albeit limited) number of suitable data available. However, our dataset is 3.5 times larger than that used previously and is more strictly filtered. A detailed discussion of the differences between the two analyses is given in the Supplementary Information.

The new and published palaeomagnetic data (87 and 109 site mean directions respectively; see Table 1) we used for this study were produced from fast-cooled igneous rock units from three continents that met strict criteria of suitability (see the Supplementary Information). We are confident that the magnetic directions used in this study represent the geomagnetic field close

to the time the rocks recording them were formed because they are associated with positive fold, conglomerate and/or baked contact tests. Reversal tests were also positive, which suggests that secular variation was adequately sampled. The PSV analysis was kept consistent as far as possible with a previous analysis of PSV in the period 0–5 Myr (ref. 9) (see the Supplementary Information).

Figure 1 plots the angular dispersion of the 2.45–2.82 Gyr virtual geomagnetic poles (VGPs) against palaeolatitude, calculated from the inclination of the mean direction assuming that the field was a geocentric axial dipole. Despite the relatively small numbers of site mean data (relative to studies focusing on more recent times), the plotted dispersions are evidently accurate enough to show a clear relationship with palaeolatitude. Furthermore, Fig. 1 shows that the basic shape of the VGP dispersion curves is extremely robust with respect to the specific details of how we carried out our analysis. Figure 1d shows our preferred dataset, which we consider to be a reliable first-order description of PSV in the late Archaean–early Proterozoic. This VGP dispersion curve is markedly different from that produced by the 0–5 Myr dataset (also shown in Fig. 1), suggesting that the nature of PSV was different in these two time periods. Specifically, the angular dispersion of VGPs from the 2.45–2.82 Gyr sites at low to mid-palaeolatitudes is lower whereas the rate of increase in VGP dispersion with palaeolatitude is slightly higher. The data used to produce the 0–5 Myr curve shown in Fig. 1 are currently being superseded by the Time Averaged Field Initiative (TAFI) project. These and other recent studies of PSV act to strengthen the conclusions of the present study, as is discussed in the Supplementary Information.

The shape of a VGP dispersion curve is dictated by several factors and is consequently difficult to interpret directly in terms of physical processes¹⁰. Nonetheless, although its physical significance is disputed, Model G (ref. 11) (see the Methods section) has proved effective at fitting the observed variations in the shapes of curves for time windows from the past 195 Myr (ref. 5) (Fig. 2a). Furthermore, the evolution of its shape parameters has been shown⁵ to correspond well to the average geomagnetic polarity reversal frequency in the particular time window for which the PSV analysis was carried out (Fig. 2), which suggests a link between mean PSV and reversal frequency. Therefore, Model G may be safely used here to describe the shapes of VGP dispersion curves, regardless of whether interpretations¹¹ of the physical significance of these shapes are correct.

The late Archaean–early Proterozoic model has both shape parameters within errors of the model fit to the Cretaceous Normal Superchron time window (point 5 in Fig. 2). Consequently, the empirical relationship shown in Fig. 2b predicts that the

Table 1 Datasets used in PSV analysis and plotted in Fig. 1. See also Supplementary Information, Fig. S2. N = number of rock units, N' of which are not rejected by the variable cutoff²³. Δ_{\max} = maximum angular distance of the non-excluded VGPs from the mean value. α_{95} = radius of circle of 95% confidence. λ = calculated palaeolatitude. S_p = total VGP dispersion. S_f = dispersion after removal of within-site dispersion. S_U and S_L are the 95% bootstrap uncertainty limits of S_f .

| Locality | Dataset | Reference | Approx age (Myr) | N | N' | Cutoff (°) | Δ_{\max} (°) | α_{95} (°) | λ (°) | S_p (°) | S_f (°) | S_U (°) | S_L (°) |
|------------|--------------------|-----------------|------------------|-----|------|------------|---------------------|-------------------|---------------|-----------|-----------|-----------|-----------|
| Matachewan | Timmins Reversed | 24 | 2,446 | 14 | 14 | 18.6 | 10.7 | 4.5 | 7.4 | 7.6 | 6.5 | 7.4 | 4.4 |
| Matachewan | Hearst | 24 | 2,446 | 10 | 10 | 21.4 | 16.5 | 8.0 | 8.2 | 9.1 | 8.6 | 12.1 | 5.5 |
| Matachewan | Chapleau East | 25 | 2,446 | 14 | 14 | 18.9 | 13.0 | 4.0 | 12.4 | 7.7 | 7.3 | 9.1 | 5.6 |
| Matachewan | Hornepayne | 24 | 2,446 | 12 | 12 | 16.7 | 11.0 | 3.7 | 13.9 | 6.5 | 6.1 | 7.1 | 3.0 |
| Nyanzian | Nyanzian | 26 | 2,823–2,780 | 10 | 10 | 20.0 | 13.5 | 6.3 | 25.0 | 8.3 | 7.0 | 8.7 | 1.5 |
| Pilbara | West Pilbara basin | This study | 2,718–2,713 | 7 | 7 | 28.6 | 20.6 | 7.2 | 27.1 | 13.1 | 12.0 | 16.8 | 8.0 |
| Pilbara | Upper | 27 & this study | 2,718–2,713 | 16 | 16 | 30.0 | 21.8 | 4.8 | 35.0 | 13.9 | 12.9 | 16.1 | 9.7 |
| Pilbara | Packages 6&7 | 27 & this study | 2,724 | 30 | 30 | 36.6 | 34.6 | 3.9 | 47.4 | 17.6 | 15.8 | 19.6 | 12.4 |
| Pilbara | Packages 1&2 | 27 & this study | 2,772–2,766 | 50 | 47 | 29.3 | 27.5 | 2.6 | 50.8 | 13.5 | 12.4 | 14.7 | 9.6 |
| Pilbara | Package 0 | This study | > 2,772 | 25 | 24 | 36.5 | 26.4 | 4.4 | 58.3 | 17.5 | 16.1 | 18.9 | 13.4 |
| Derdepoort | Derdepoort | 28 | 2,782 | 8 | 8 | 49.6 | 36.3 | 9.2 | 64.6 | 24.8 | 24.1 | 24.2 | 18.4 |
| Matachewan | Group 1* | 24 | 2,446 | 24 | 24 | 19.5 | 16.2 | 3.8 | 7.7 | 8.1 | 7.2 | 9.0 | 5.7 |
| Matachewan | Group 2* | 24,25 | 2,446 | 32 | 32 | 18.3 | 13.0 | 2.6 | 13.8 | 7.4 | 6.9 | 8.2 | 5.5 |
| Pilbara | Lower Group* | 27 & this study | 2,772–2,721 | 80 | 75 | 30.7 | 28.7 | 2.2 | 49.5 | 14.3 | 12.8 | 14.7 | 10.8 |

*Matachewan Group 1 comprises Timmins Reversed and Hearst sites rotated onto common mean declination. Group 2 comprises Chapleau East and Hornepayne datasets, together with six normal polarity sites from Timmins locality. Pilbara Lower Group comprises Packages 1&2 and Packages 6&7.

2.45–2.82 Gyr period was characterized by a paucity of geomagnetic reversals relative to the majority of time windows in the period 0–195 Myr (which had a combined average reversal frequency of $\sim 2.6 \text{ Myr}^{-1}$). This is consistent with the small number of reversals observed in the palaeomagnetic records of the Pilbara (only four reversals found in sections spanning at least 17 Myr) and Matachewan (one reversal found in a period likely to exceed 30 Myr), as well as the low reversal frequency ($\sim 0.2 \text{ Myr}^{-1}$) recently estimated⁴ for the period 1.05–2.77 Gyr.

While the records that comprise our Archaean–Proterozoic VGP dispersion curve do not provide coverage for the whole of the 380 Myr interval from which they are drawn, their combined length of ~ 130 Myr is a considerable fraction of it. It is therefore intriguing that the shape of this curve is similar to one from a period lasting just 30 Myr at the extreme end of the range of geomagnetic variation observed for the past 195 Myr. A composite VGP dispersion curve was used to obtain average Model G parameters for the entire period 0–195 Myr (see the Methods section). These indicated that the average PSV during this time was similar to that in the 0–5 Myr subperiod but significantly different from that in the 2.45–2.82 Gyr period (Fig. 2a). While shape parameter b for the 2.45–2.82 Gyr model is within errors of that of both the 0–5 Myr and the mean 0–195 Myr models, its shape parameter a is different at the 95% confidence level. Two further tests for the significance of this difference are provided in the Supplementary Information and both produce positive results. We therefore conclude that, in terms of its expression in VGP dispersion curves, average geomagnetic secular variation in the late Archaean and earliest Proterozoic was fundamentally different from that occurring in the past 195 Myr.

The empirical relationship shown in Fig. 2b suggests that the geodynamo was, on average, in a more stable state (that is, less susceptible to reversals, all else being equal) in the period 2.45–2.82 Gyr than it was in the period 0–195 Myr. Furthermore, this relationship recently received support from a study⁴ comparing the spatial energy distributions of eight self-consistent dynamo simulations (see the Methods section for explanation).

Changes in mean VGP dispersion curves, like changes in mean geomagnetic reversal frequency, cannot unequivocally be associated with any particular forcing factor and may even occur spontaneously¹². The variations observed in the reversal record for the past 200 Myr as well as the identification of two older superchrons (the Kiaman at 260–312 Myr and the recently

established¹³ Moyero at 460–490 Myr) suggest some modulation of geomagnetic behaviour on a timescale of ~ 200 Myr. This has been taken by some^{14,15} as an indication that mantle processes are forcing the geodynamo; whether this is true or not, we found that the observed differences between average PSV in the periods 0–195 Myr and 2.45–2.82 Gyr are very unlikely to be caused by variations with a period of 200 Myr or shorter.

There are no obvious forcing mechanisms that would produce variations in geomagnetic behaviour with periods both longer than that observed in the reversal record and shorter than the time between the two intervals studied here. We therefore expect that our observations represent the limits of a single evolution towards decreased stability; it will be for future studies to verify this and to determine whether the transition between these limits was continuous or abrupt.

It is plausible that the same process that produced the Cretaceous Normal Superchron was responsible for the apparent high level of geodynamo stability observed in the late Archaean—early Proterozoic. However, the period of time the Cretaceous Normal Superchron represents is just 15% of the past 200 Myr, whereas the field was in a highly stable state for a significantly larger proportion of the time in the Archaean–Proterozoic (see the Supplementary Information). If the same process was responsible then it must have had a much longer associated time period in the Archaean–Proterozoic. Instead, we suspect that an altogether different process caused the implied decrease in average stability between then and now.

One of the dominant factors affecting the geodynamo over timescales exceeding 10^9 yr is likely to be the growth of the inner core. This process is the principal source of power to the geodynamo^{16,17} and is also responsible for progressively changing the geometry of the shell in which the geodynamo operates. While the timing of the inner core's formation remains a highly contentious issue^{18–20}, it is reasonable to assume that its influence on the geodynamo was substantially less during the late Archaean–early Proterozoic than it is today. Even the most conservative of thermal models²¹ (giving a nucleation age of 3.9 Gyr) implies that its radius was less than 70% of its current value at 2.7 Gyr, whereas other models^{18,21} predict that it was unlikely to have formed at all. The magnetic diffusion time of the inner core is proportional to the square of its radius and was therefore less than 50% of its present-day value. Earth's rotation rate was also increased at this time and may have been as much as 40% higher at 2.45 Gyr (ref. 22).

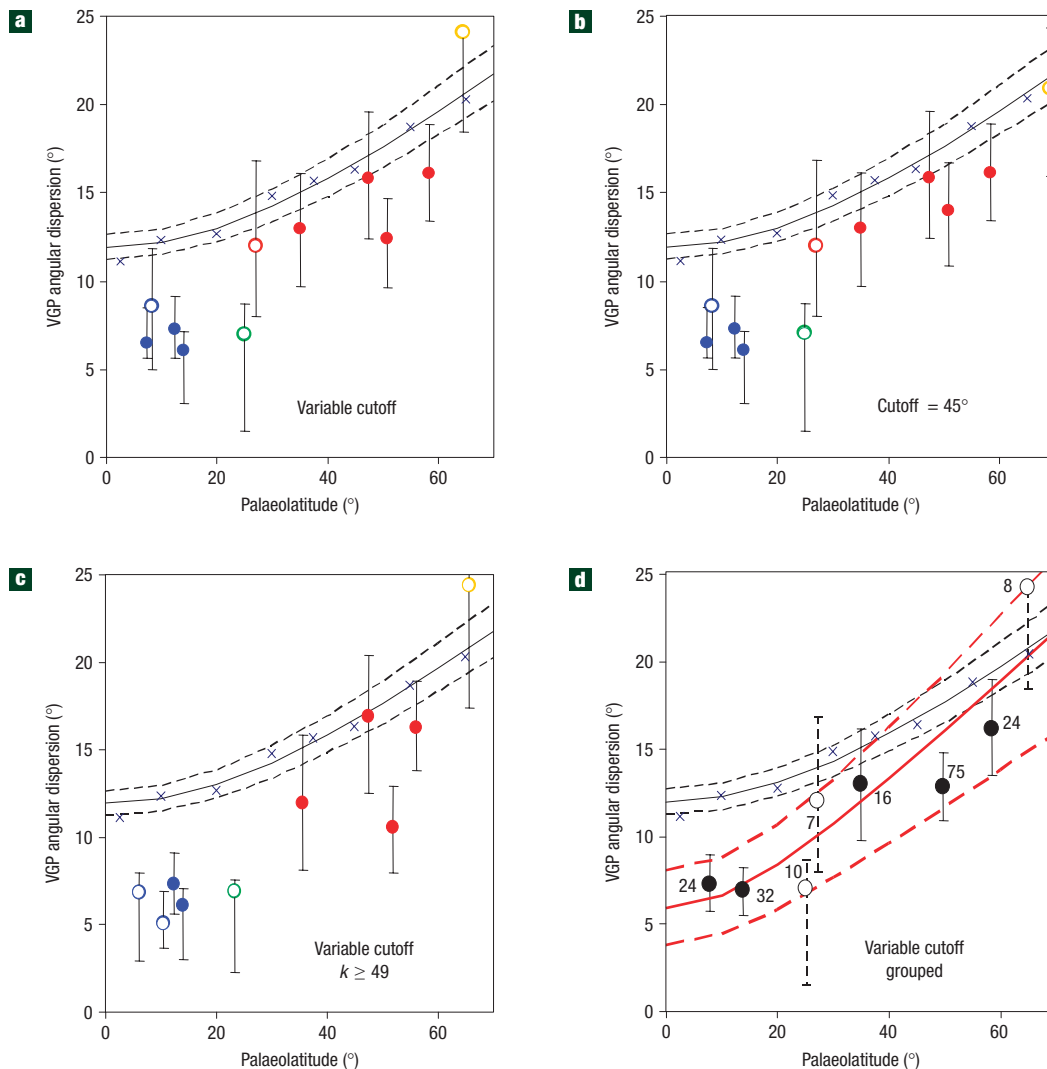


Figure 1 VGP dispersion plots for the periods 2.45–2.82 Gyr and 0–5 Myr. Circles represent datasets shown in Table 1: blue, Matachewan^{24,25}; green, Nyanzian²⁶; red, Pilbara²⁷; yellow, Derdepoort²⁸, filled, $N > 10$. Error bars are 95% bootstrap estimates. Crosses represent the highest-quality datasets from 0–5 Myr (ref. 9) with Model G (ref. 11) (black line) fitted to them and 95% uncertainty (bootstrap method) limits shown as dashed lines. The panels show the effects of different analytical approaches (see the Supplementary Information). The red curve in **d** shows Model G fitted to the 2.45–2.82 Gyr data. Values of N are shown.

Roberts and Glatzmaier⁷ compared three different numerical simulations of the geodynamo with different inner-core radii (as well as rotation rates and core heat fluxes). In contrast to what was expected, they found that the time dependence of the field and its deviation from axial symmetry were positively related to the radius of the inner core. They concluded that a larger inner core may promote instability by enabling different parts of the fluid outer core to generate the field with greater independence from one another. This occurs both because the ratio of the outer-core volume to its depth is increased and because the inner core presents a greater physical barrier to large-scale flow structures in the outer core. Particularly consistent with the present study's findings was the observation⁴ that in the simulation run with an inner core of 25% of today's radius an especially high ratio of antisymmetric-to-symmetric spherical harmonic terms (that is, high b/a in Model G terms—see the Methods section) was produced, indicating that the dynamo was unusually stable.

In terms of its mean secular variation, averaged over hundreds of Myr, our findings suggest that the geodynamo has become less

stable over the past few billions of years; this trend may well persist as the inner core continues to grow. It is conceivable that the reduced diffusion time of a smaller inner core compensated for the less erratic field so that the probability of polarity reversal was not reduced from its present value. However, our limited knowledge of Precambrian paleomagnetism is consistent with a significantly reduced reversal frequency at this time.

METHODS

Model G (ref. 11) is given by $S = (a^2 + (b\lambda)^2)^{1/2}$, where S is the VGP angular dispersion, λ is palaeolatitude and a and b are constants defined as the shape parameters of the curve. The best fit of Model G to VGP dispersion data was obtained using the least-squares method, and 95% confidence limits were obtained using a bootstrap approach. The resulting shape parameters are for the 0–5 Myr curve $a = 11.9 \pm 0.7$, $b = 0.26 \pm 0.02$, and for the 2.45–2.82 Gyr curve shown in Fig. 1d $a = 5.9 \pm 2.1$, $b = 0.30 + 0.05 - 0.08$. The composite VGP dispersion curve for the period 0–195 Myr (large filled circles in Fig. 2) was obtained by plotting all the binned dispersion estimates given in Tables 2–7 of ref. 5 together on the same plot (see Supplementary Information, Fig. S3).

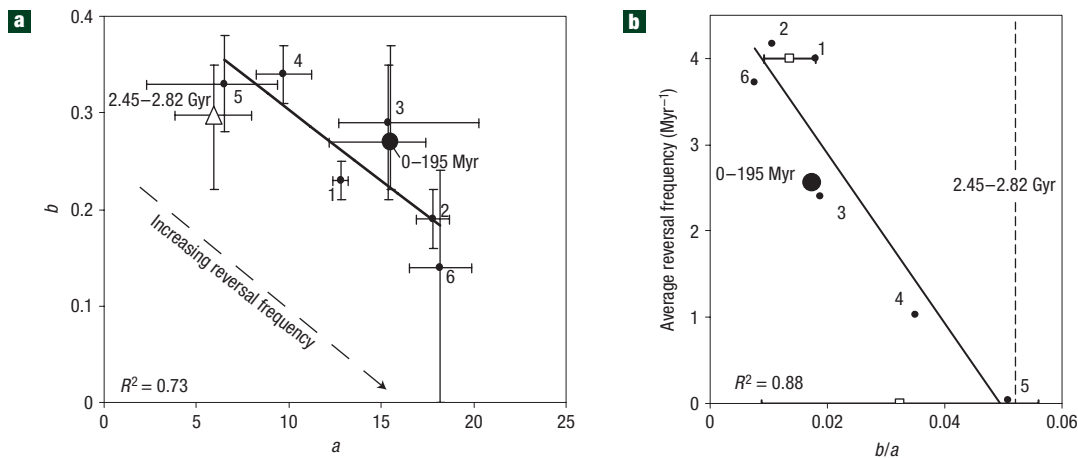


Figure 2 Comparison of PSV in the periods 2.45–2.82 Gyr and 0–195 Myr. **a**, Shape parameters of Model G (ref. 11) fitted to VGP dispersion curves from time windows 0–5 Myr (1), 5–22.5 Myr (2), 22.5–45 Myr (3), 45–80 Myr (4), 80–110 Ma (5) and 110–195 Myr (6). The triangle is the red curve in Fig. 1d; the large filled circle is the composite 0–195 Myr curve (see the Methods section). **b**, Relationship with geomagnetic reversal frequency (predicted to be very low for the 2.45–2.82 Gyr period). Squares relate to more recent studies^{29,30} (see the Supplementary Information). Lines in both plots are linear regressions fitted to points 1–6. Error bars are 95% confidence limits obtained using the bootstrap approach.

We then attached a weight to each point according to the length of the time window from which it was derived and fitted a Model G curve to the plot as normal. This represents an ‘average’ model for the entire period, in the sense that it estimates the curve that would be measured if rocks with ages distributed throughout the period 0–195 Myr were sampled equally. It has shape parameters $a = 15.5 + 1.9 - 3.3$, $b = 0.27 + 0.10 - 0.05$. An alternative means of calculating this average 0–195 Myr model is described in the Supplementary Information, and produced similar results to that described here.

The shape parameter a of Model G is argued¹¹ to represent the variation of the equatorially symmetric part of the field whereas the shape parameter b represents the equatorially antisymmetric components. A recent study⁴ comparing the spatial energy distributions of eight self-consistent geodynamo simulations found that their ratios of equatorially-antisymmetric-to-symmetric spherical harmonic terms correlated inversely with their tendency to reverse; this constitutes theoretical support for the relationship shown in Fig. 2b.

Received 17 October 2007; accepted 18 March 2008; published 4 May 2008.

References

- Gubbins, D. The distinction between geomagnetic excursions and reversals. *Geophys. J. Int.* **137**, F1–F3 (1999).
- Hollerbach, R. & Jones, C. A. Influence of the earth's inner-core on geomagnetic fluctuations and reversals. *Nature* **365**, 541–543 (1993).
- Roberts, N. & Piper, J. D. A. in *Geomagnetism* (ed. Jacobs, J. A.) 163–260 (Elsevier, New York, 1989).
- Coe, R. S. & Glatzmaier, G. A. Symmetry and stability of the geomagnetic field. *Geophys. Res. Lett.* **33**, 2006GL027903 (2006).
- McFadden, P. L., Merrill, R. T., McElhinny, M. W. & Lee, S. H. Reversals of the earth's magnetic-field and temporal variations of the dynamo families. *J. Geophys. Res.* **96**, 3923–3933 (1991).
- Morrison, G. & Fearn, D. R. The influence of Rayleigh number, azimuthal wavenumber and inner core radius on 2–1/2 D hydromagnetic dynamos. *Phys. Earth Planet. Inter.* **117**, 237–258 (2000).
- Roberts, P. H. & Glatzmaier, G. A. The geodynamo, past, present and future. *Geophys. Astrophys. Fluid Dyn.* **94**, 47–84 (2001).
- Smirnov, A. V. & Tarduno, J. A. Secular variation of the late Archean early Proterozoic geodynamo. *Geophys. Res. Lett.* **31** doi:10.1029/2004GL020333 (2004).
- McElhinny, M. W. & McFadden, P. L. Palaeosecular variation over the past 5 Myr based on a new generalized database. *Geophys. J. Int.* **131**, 240–252 (1997).
- Hulot, G. & Gallet, Y. On the interpretation of virtual geomagnetic pole (VGP) scatter curves. *Phys. Earth Planet. Inter.* **95**, 37–53 (1996).
- McFadden, P. L., Merrill, R. T. & McElhinny, M. W. Dipole quadrupole family modeling of paleosecular variation. *J. Geophys. Res.* **93**, 11583–11588 (1988).
- Hulot, G. & Gallet, Y. Do superchrons occur without any palaeomagnetic warning? *Earth Planet. Sci. Lett.* **210**, 191–201 (2003).
- Pavlov, V. & Gallet, Y. A third superchron during the Early Paleozoic. *Episodes* **28**, 78–84 (2005).
- Courtillot, V. & Olson, P. Mantle plumes link magnetic superchrons to Phanerozoic mass depletion events. *Earth Planet. Sci. Lett.* **260**, 495–504 (2007).
- McFadden, P. L. & Merrill, R. T. History of earth's magnetic-field and possible connections to core–mantle boundary processes. *J. Geophys. Res.* **100**, 307–316 (1995).

- Gubbins, D., Alfe, D., Masters, G., Price, G. D. & Gillan, M. J. Can the Earth's dynamo run on heat alone? *Geophys. J. Int.* **155**, 609–622 (2003).
- Labrosse, S. Thermal and magnetic evolution of the Earth's core. *Phys. Earth Planet. Inter.* **140**, 127–143 (2003).
- Lassiter, J. C. Constraints on the coupled thermal evolution of the Earth's core and mantle, the age of the inner core, and the origin of the (OS)-O-186/(OS)-O-188 ‘core signal’ in plume-derived lavas. *Earth Planet. Sci. Lett.* **250**, 306–317 (2006).
- Brandon, A. D. & Walker, R. J. The debate over core–mantle interaction. *Earth Planet. Sci. Lett.* **232**, 211–225 (2005).
- Christensen, U. R. & Tilgner, A. Power requirement of the geodynamo from ohmic losses in numerical and laboratory dynamos. *Nature* **429**, 169–171 (2004).
- Buffett, B. A. Estimates of heat flow in the deep mantle based on the power requirements for the geodynamo. *Geophys. Res. Lett.* **29** doi:10.1029/2001GL014649 (2002).
- Williams, G. E. Geological constraints on the Precambrian history of earth's rotation and the moon's orbit. *Rev. Geophys.* **38**, 37–59 (2000).
- Vandamme, D. A new method to determine paleosecular variation. *Phys. Earth Planet. Inter.* **85**, 131–142 (1994).
- Bates, M. P. & Halls, H. C. Broad-scale proterozoic deformation of the central superior-province revealed by paleomagnetism of the 2.45 Ga Matachewan dyke swarm. *Can. J. Earth Sci.* **28**, 1780–1796 (1991).
- Halls, H. C. & Palmer, H. C. The tectonic relationship of two early proterozoic dyke swarms to the Kapuskasing structural zone: A paleomagnetic and petrographic study. *Can. J. Earth Sci.* **27**, 87–103 (1990).
- Meert, J. G., Van der Voo, R. & Patel, J. Paleomagnetism of the Late Archean Nyanzian System, Western Kenya. *Precamb. Res.* **69**, 113–131 (1994).
- Strik, G. H. M. A., Blake, T. S., Zegers, T. E., White, S. H. & Langereis, C. G. Palaeomagnetism of flood basalts in the Pilbara Craton, Western Australia: Late Archean continental drift and the oldest known reversal of the geomagnetic field. *J. Geophys. Res.* **108**, EPM 2-1–EPM 2-21 (2003).
- Wingate, M. T. D. A palaeomagnetic test of the Kaapvaal–Pilbara (Vaalbara) connection at 2.78 Ga. *South African J. Geol.* **101**, 257–274 (1998).
- Tarduno, J. A., Cottrell, R. D. & Smirnov, A. V. The Cretaceous superchron geodynamo: Observations near the tangent cylinder. *Proc. Natl Acad. Sci. USA* **99**, 14020–14025 (2002).
- Johnson, C. L. *et al.* Recent investigations of the 0–5 Ma geomagnetic field recorded by lava flows. *Geochem. Geophys. Geosyst.* doi:10.1029/2007GC001696 (in the press, 2008).

Supplementary Information accompanies this paper on www.nature.com/naturegeoscience.

Acknowledgements

This research was undertaken with funding provided by the Netherlands Science Foundation (NWO) and conducted under the programme of the Vening Meinesz Research School of Geodynamics (VMSG).

Author contributions

A.J.B. undertook the paleosecular variation analyses and provided the interpretation. G.H.M.A.S. obtained the newly reported data from the Pilbara Craton and undertook PSV analyses on these. C.G.L. initiated the project and advised and assisted throughout.

Author information

Reprints and permission information is available online at <http://npg.nature.com/reprintsandpermissions>. Correspondence and requests for materials should be addressed to A.J.B.

NGS2007-10-00289A

SUPPLEMENTARY INFORMATION

SuppInfo.pdf

PDF format

Supplementary Information

New Palaeomagnetic Directional Data

The new palaeomagnetic measurements used in this study are from the same packages (primarily comprised of flood basalts) of the Nullagine and Mount Jope Supersequences (Pilbara Craton, Western Australia) as previously published data¹ which were also used. However, whereas the previous data were taken from rocks outcropping in the Nullagine syncline and the Meentheena Centrocline, the 92 new sites were obtained from other regions of the East Pilbara Basin as well as the Meentheena and West Pilbara basins (Supplementary table 1). Detailed information about the sampling areas and individual sites is given elsewhere^{2,3}.

Core samples were generally taken in the field using a petrol engine drill and orientated with both a magnetic and sun compass. In the laboratory, both thermal and AF demagnetisation was used and the NRM was measured on a 2G Enterprises DC-SQUID cryogenic magnetometer or occasionally on an AGICO JR5 spinner magnetometer. NRM directions were analysed and interpreted with Zijderveld diagrams⁴. Principal component analysis⁵ was used to determine the directions of the various NRM components and components with maximum angular deviation (MAD) more than 10° were not accepted.

The demagnetisation behaviour of the new samples was generally consistent with that observed in their previously published counterparts¹. The low temperature component was frequently aligned close to the present-day field but was usually removed by thermal demagnetisation to approximately 300°C. A previously observed¹ medium temperature component with unblocking temperature up to 480°C was observed in samples from Packages 1, 2, 7, 8, and 10. The convergent high temperature (HT) component was again taken as the primary. It was used effectively to check the correlation of the packages across the basins³; Supplementary table 1 gives the package mean directions and supplementary figure 1 provides some examples of Zijderveld plots (including some that were not accepted).

Detailed bedding plane measurements were made at the outcrops. The tectonic corrections resulting from these tended to be small (supplementary table 1) as the folding of these flood basalts was generally slight. One exception to this was Package 0 which represents locally folded (up to 74°) flood basalts of unknown age below Package 1 which were sampled in the Marble Bar Basin. The HT component of this package passes a fold test which demonstrates that it has an age older than Package 1 (2772 ± 2 Ma). It was previously observed¹ that units in Package 2 in the Nullagine syncline and the Meentheena Centrocline were reversed with respect to older and younger packages. We also observed this in the areas we sampled and performed a reversal test between the mean direction of Package 2 with Packages 1 and 6. Both of these tests gave positive results with classification B⁶. In addition to this reversed period, we also found evidence for a later short reversed period at ~2721 Ma when Package 7 was emplaced. The evidence for this consisted of reversed HT components measured in a single lava flow in the Boodalyerri Creek Area and in a pair of Package 7-related sills in the West Pilbara Basin. The slower-cooled nature of these sills allows a reversal test to be performed using individual directions rather than site means. The 15 reversed directions were tested against 13 directions taken from two sills directly beneath these. This reversal test also passed with classification B.

Analysis of Palaeosecular variation: methodology

The methodology for our PSV analysis was based on that outlined by previous studies⁷⁻¹⁰. In particular, we aimed to be as consistent as possible with a previous detailed analysis of the 5-0 Ma dataset⁸.

To qualify for inclusion in our analysis, datasets were required to meet the following criteria:

1. A minimum age of the rock units exceeding 2.4 Ga
2. Results produced from igneous rock units which are extrusive or high-level intrusive with explicit mention of sampling concentrated at the rapidly-cooled margins.
3. A minimum number of 7 sites (each one an individual rock unit) per dataset with no suggestion of latitudinal drift having occurred between the emplacement of the various rock units
4. Mean directions at each site comprise measurements from at least three independently-oriented samples with an associated $\alpha_{95} < 20^\circ$
5. Positive field tests demonstrating that the age of the magnetisation is the same or close to that of the rock unit.
6. Zijderveld diagrams⁴ and principal component analysis⁵ used to analyse the data.

Supplementary figure 2 shows the distribution of VGPs for the 11 datasets used in this study. Prior to calculating the angular dispersion of the VGPs, a variable cut-off¹¹ was applied to exclude any data recording either an excursionsal field or affected by some measurement error. This affected only 2 of our 11 datasets. We also tested a less stringent, fixed cutoff (requiring VGP latitude to be less than 45° from the mean pole) (figure 1b) to demonstrate that our choice of cutoff does not affect our conclusions. Finally, we tested the effects of a stricter precision criterion (figure 1c) and made the same observation.

To constrain the relationship between VGP dispersion and palaeolatitude further, we grouped datasets wherever their ages and palaeolatitudes were indistinguishable (table 1; figure 1d). This process also left the basic shape of the VGP dispersion curve unchanged.

The total angular dispersion S_p of the set of N VGPs was calculated from:

$$S_p = \left(\frac{1}{N-1} \sum_{i=1}^N \Delta_i^2 \right)^{1/2} \quad (1)$$

where each pole is an angular distance Δ_i away from the mean of the dataset.

It is necessary to extract the dispersion produced solely by the geomagnetic field (S_F) from the total (S_p) which is also a product of random errors associated with the measurement (S_W):

$$S_F^2 = S_p^2 - (S_W^2 / n_{\text{avg}}) \quad (2)$$

To retain consistency with a previous study⁸, we estimated the error term using the mean value of α_{95} for the dataset:

$$\frac{S_w^2}{n_{avg}} = 0.335 \bar{\alpha}_{95}^2 \frac{2(1 + 3 \sin^2 \lambda)^2}{(5 + 3 \sin^2 \lambda)} \quad (3)$$

Supplementary table 2 and figure 1 shows the values of S_F and their associated 95% uncertainty bounds produced using the bootstrap method.

Where palaeomagnetic directions are taken from proximate lava flows, there exists the danger of over-representing the field at certain time intervals and therefore of underestimating PSV¹². We wished to ensure that this process was not responsible for the low VGP dispersion measurements made from some of the lavas used in this study. We tested this by grouping site mean directions which were indistinguishable using the common true mean direction test¹³ and which were produced from sites within 1 km of one another. This approach to similar-field grouping is very likely to be over-strict so we would expect it to exaggerate any possible effect. Nonetheless, observed differences in the measured VGP dispersions were generally negligible and the maximum increase produced by these reductions was less than 1.5°. This suggests that our measurements were not strongly influenced by bursts of rapid lava emplacement. Additionally, it is worth noting that the 5-0 Ma dataset which we are using for comparison⁸ also did not employ any such approach. Further discussion over the adequacy of secular variation sampling is given below.

Analysis of Palaeosecular variation: discussion of datasets

The Matachewan data were taken from the published datasets of 2 studies^{14,15}. The complex tectonic history of these dykes has already been studied in detail^{16,17}. The palaeomagnetic data used in this study were taken exclusively from dykes from outside the Kapuskasing Structural Zone which cooled relatively quickly and have been shown (using baked contact tests) to record a primary remanence. The two studies from which the data were taken both made explicit mention of sampling being concentrated in the chilled margins where the time to cool through the blocking temperatures is not expected to exceed a few weeks¹⁸. This is important as the average thickness of the dykes is 20 m. Bedding plane measurements were not possible and therefore no tectonic corrections were made to these data. This is permissible because the observed verticality of the dykes and the consistency of directions measured in dykes from the same localities implies that folding was very slight. Furthermore, the low VGP scatters and magnetic inclinations measured from these dykes implies that any uncorrected tilting of the dykes would only serve to strengthen the conclusions reached by this study (by decreasing the scatter and/or increasing the palaeolatitude). Some large-scale vertical-axis rotations between localities were implied by the palaeomagnetic directions¹⁴ and were taken into account as will be discussed below.

Data was derived from dykes from four localities each spanning several tens of kilometres¹⁴. The duration of emplacement for the entire Matachewan swarm is thought to exceed 30 Myr¹⁷ and we are confident that the low VGP scatter recorded by these

dykes was not produced by inadequate time-sampling of the field. The mean palaeomagnetic directions produced from the localities have been shown to be consistent with the structural setting and to indicate latitudinal plate motion^{14,16,17} which suggests that secular variation has been largely averaged out. A single polarity reversal (from reversed to normal) is implied to have occurred over the time that the sampled dykes were emplaced¹⁷.

The mean directions of the reversely magnetised dykes at Timmins (14 dykes) and Hearst (10 dykes)¹⁴ recorded indistinguishable palaeolatitudes but inferred a relative rotation of 12°. In order to merge the data into Group 1 (see figure 1d and table 1), we corrected for this.

Six younger, normally magnetised dykes in the Timmins locality had a consistent declination with the reversely magnetised dykes there, indicating that a rotation correction could be safely undertaken despite their small number. The palaeolatitude given by these normally magnetised dykes was consistent with that of 14 other normally-magnetised dykes at Chapleau East¹⁵ and 12 reversely magnetised dykes at Hornepayne¹⁴ (which were corrected for 12 and 4° of relative rotation respectively). Together these comprised the Matachewan Group 2 dataset in table 1.

The Nyanzian dataset comprised palaeomagnetic directions from extrusive rocks (basalts, rhyolites, and andesites) from the Tanzanian Craton in Western Kenya¹⁹. The age of this Nyanzian system has recently been refined to ca. 2780 to 2823 Ma²⁰ and the age of the magnetisation is constrained to $> 2472 \pm 30$ Ma by positive fold, conglomerate, and reversal tests¹⁹. The passage of the latter field test suggests that this dataset is likely to sample secular variation adequately.

The Pilbara dataset consisted of a total of 128 (including 87 new) site mean directions that passed the selection criteria outlined above. These were drawn from flood basalts emplaced in eight distinct ‘packages’ over a total period of time exceeding 57 Myr (> 2772 - 2715 Ma²¹). However, the minimum combined length of time of emplacement of the units from which we obtained reliable palaeomagnetic data is approximately 17 Myr²¹ for which we observed four polarity reversals.

The Pilbara data was split into four sets with distinct palaeolatitudes for the PSV analysis (table 1). Package 0 was the oldest (> 2772 Ma) and was associated with a positive fold test. Packages 1 and 2 passed a reversal test (suggesting adequate sampling of secular variation) and Packages 6 and 7 had indistinguishable mean directions from one another and a palaeolatitude consistent with Packages 1 and 2. Some 29° of relative rotation is inferred to have had occurred after Packages 1 and 2 were emplaced but before the emplacement of Packages 6 and 7. Therefore, the directions from these two sets were rotated so that they shared a common mean before being combined into the Pilbara Lower Group (c. 2772-2721 Ma) shown in table 1. In addition to the reversal tests performed between Packages 1 and 2 and within Package 7, rocks from Package 1 also produced positive fold and conglomerate tests^{1,3}.

Mean directions from Packages 8, 9, and 10 cropping out in the East Pilbara basin were grouped into the Upper dataset (supplementary table 2). The same packages thought to be cropping out in the West Pilbara Basin gave different directions and were treated separately.

The final dataset used in this analysis were produced from a sequence of basaltic lava flows of the Derdepoort Belt of South Africa²². Although a fold test was ambiguous,

a positive conglomerate test strongly suggests that these magnetisations are as old as the rocks themselves (2782 ± 5 Ma).

A comparison with a previous study of palaeosecular variation in the late Archaean-early Proterozoic

A previous study²³ concluded that PSV in the late Archaean / early Proterozoic was, within errors, the same as in the last 5 Myr with a suggestion of a slightly reduced equatorially symmetric family. It is instructive to explain the differences in that analysis from this one which were responsible for the much stronger conclusion reached by the present study. Smirnov & Tarduno²³ used three datasets for their PSV analysis. One of these was from ~2.5 Ga Karelian dykes²⁴ which we did not use on account of it failing our criterion 2 (see above). However, had we used this set, it would have supported our central conclusion. Their quoted VGP dispersion was 11.8° (for a palaeolatitude of 27°) but this decreases to 9.4° when we apply criterion 4 above to the data and when we correct for within-site error (which they did not). This new value is highly consistent with the model fit to our data that is shown in figure 1d.

The Pilbara dataset they used¹ was equivalent to our Pilbara Lower Group (table 1) but just one-third of the size on account of the new data we incorporate here. They measured almost precisely the same VGP dispersion as we did (14.3°) but did not correct their value for within-site scatter which brought our calculated dispersion down to 12.8° .

The difference in VGP scatter they record for the Matachewan dyke swarm is a result of the difference in the size of the datasets. Their dataset is 15 site mean directions from 2 localities whereas ours is 56 site mean directions from 4 localities. We did not include their 15 data in our analysis on account of them failing our criterion 2 above. However, it is instructive to perform an explicit comparison of their data with those used here. One of their localities (the same as our Hornepayne locality) produced 8 passing site mean directions which gave an angular dispersion of $(8.7 +0.9/ -3.6)^\circ$, consistent with the conclusions of this study. Their other locality was Chapleau-Central (in the nomenclature of Bates & Hall, 1991¹⁴) where 7 site mean directions gave an angular dispersion of $(11.8 +4.9/ -3.5)^\circ$. Halls & Palmer (1990)¹⁵ also produced a high angular dispersion $(11.3 +4.2/ -3.2)^\circ$ from dykes of this area but we did not include this measurement because it comprised only 5 site mean directions. Therefore, in terms of individual locality data, there is no inconsistency between the results produced by Smirnov & Tarduno and the data used in this study. Smirnov & Tarduno rotated and combined the data from their two localities and obtained a VGP angular dispersion of 10.8° . If their data had of been included in this study, then it would have been incorporated into our Matachewan Group 2 dataset (Table 1). We tested the effects of doing this and found that the total measured angular dispersion of Group 2 was raised by just 0.9° (and only 0.5° after the variable cutoff was applied). This would have had a negligible effect on the model we calculated (displayed in figure 1d) and no effect on the conclusions of the study.

The present study also uses two datasets from African extrusive rocks which the previous study did not. Though these each comprise relatively few site mean directions, they are of good quality, they pass field tests, and they are altogether inconsistent with the previous study's conclusions of similar PSV in the 5-0 Ma and 2.45 – 2.80 Ga

periods. To summarise, it is clear that the differences in the conclusions of the two studies are caused purely by the present study employing a larger overall dataset together with stricter selection criteria and a within-site error correction.

Testing the robustness of the observed differences in VGP dispersion curves

The different VGP dispersion curves reported by McFadden et al.²⁵ suggest that the geomagnetic field underwent a large amount of variation in its mode of PSV during the period 0-195 Ma. If the field was similarly variable during the period 2.45-2.82 Ga, then our VGP dispersion curve shown in figure 1d may not be a good representation of the average behaviour for the entire period. In this section we show that, while we cannot be certain how well our 2.45-2.82 Ga data represent the underlying distribution of VGP dispersion data for the entire period, we can be confident that this distribution is different to that underlying the McFadden et al data for the period 0-195 Ma.

Supplementary Figure 3 shows that the VGP dispersions associated with the Matachewan and Nyanzian data are unquestionably lower than that obtained for any sub-period from the last 195 Myr except perhaps the period 80-110 Ma which incorporates the Cretaceous Normal Superchron (CNS). This sub-period constitutes some 15% of the total period 0-195 Ma so, if the underlying distribution of VGP dispersion data in this period and in 2.45 - 2.82 Ga were the same, the likelihood of obtaining two temporally and spatially independent measurements at random which were both from a superchron would be $0.15 \times 0.15 = 0.02$. On this basis, the 2.45-2.82 Ga VGP dispersion data appears distinct from the 0-195 Ma data at the 95% confidence level. Furthermore, we can conclude that the field was very likely in a 'superchron-like state' for significantly longer than 15% of the length of the 2.45-2.82 Ga period

A further test for significance was carried out using the Model G parameters originally assigned to the 0-195 Ma sub-periods by McFadden et al.²⁵. For every palaeolatitude recorded by the 7 Archaean-Proterozoic data shown in supplementary figure 3 (and figure 1d), an age between 0 and 195 Ma was randomly chosen and a mean value of VGP dispersion was then calculated from the associated model. We then drew a simulated value of VGP dispersion from a Gaussian distribution with the calculated mean and with variance determined from the mean of the 95% confidence limits which were supplied by McFadden et al. Model G was then fit, using the least squares method, to the 7 points calculated thus and its a and b parameters were recorded. A total of 10,000 repetitions of this process produced mean model parameters ($a = 14.6 + 3.3 / - 4.3$, $b = 0.25 \pm 0.09$) which were similar to those obtained using an empirical estimate of the mean 0-195 Ma curve (see 'Methods' section of main text). Only 0.1% of the simulated curves had an a parameter as low as that (5.9) of the model fit to the original Archaean-Proterozoic data. This implies a significant difference in the distributions of the dispersion data for the two periods at the 99.9% confidence level.

The implications of recent studies performed on PSV in the period 0-200 Ma

Johnson et al²⁶ very recently produced an updated record of VGP dispersion in the 0-5 Ma period using a much higher quality dataset than was available to McElhinny & McFadden⁸. Their binned data (combined on the same hemisphere) is shown in supplementary figure 4a alongside our data for the period 2.45-2.82 Ga. The new data has higher VGP dispersion at lower latitudes than does the older data from the same time period (also shown). Consequently, our case for PSV being different in the periods 2.45-2.82 Ga and 0-5 Ma is strengthened by the introduction of the new data.

The *b/a* ratio of the Model G fit to this new VGP dispersion curve is plotted against reversal frequency in figure 2b of the main text (empty square). Also shown there is the *b/a* ratio of the Model G fit to an updated study of the Cretaceous Normal Superchron undertaken by Tarduno et al²⁷. The large error bars were produced by the bootstrap method as a consequence of the model being fit to only four points.

The results of a recently submitted analysis²⁸ of VGP dispersion in the Cretaceous Normal Superchron and in the Jurassic period (144-200 Ma) are summarised in supplementary figure 4b. These confirm the qualitative relationship between PSV and reversal frequency reported by McFadden et al. but suggest that PSV may not have been as dramatically different in the CNS (relative to that in 0-5 Ma period) as originally thought. This would imply that PSV in the 2.45-2.82 Ga period was, in fact, in a much more stable configuration than in the CNS and therefore strengthens the conclusions of this study considerably.

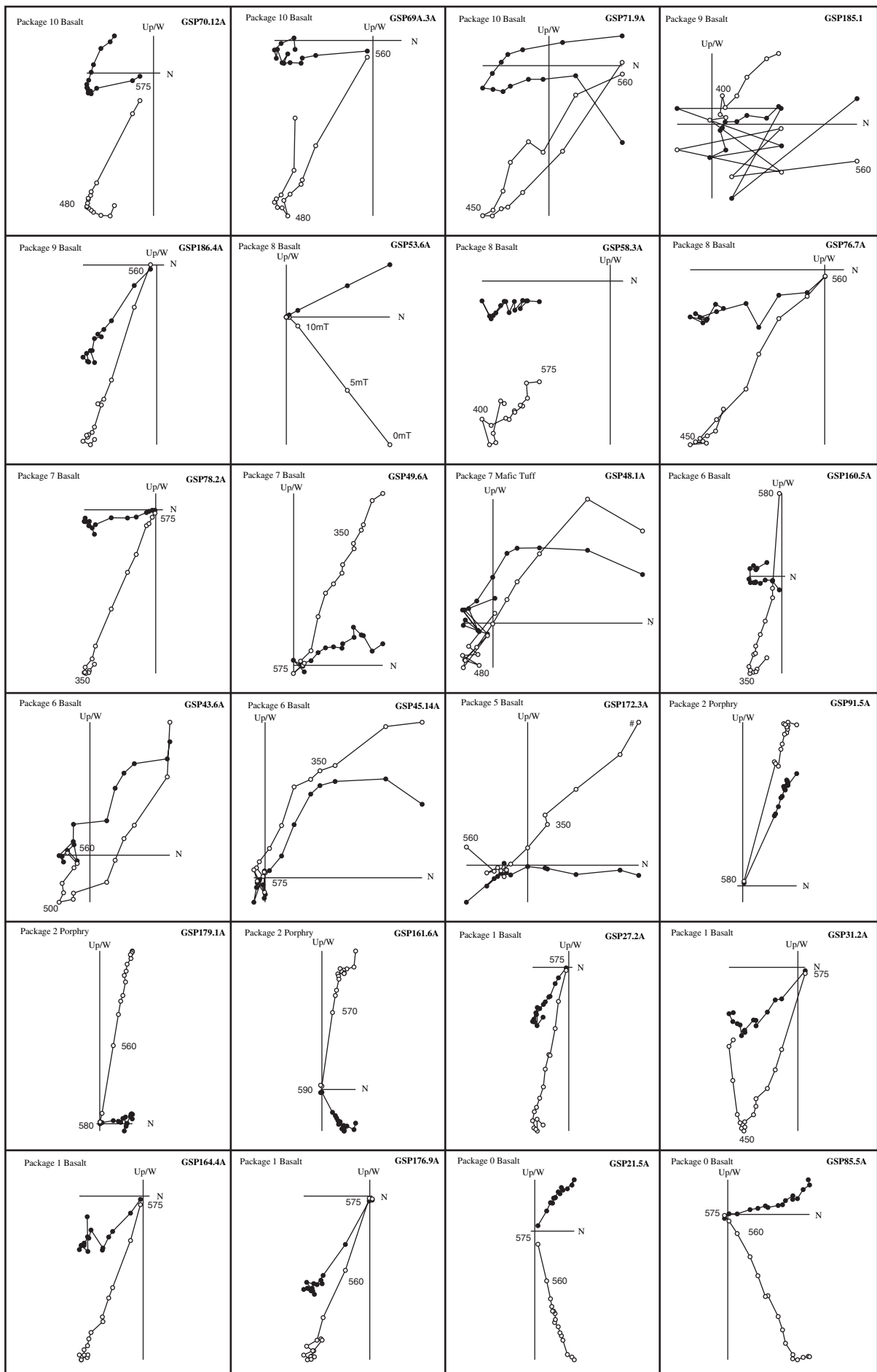
The submitted study of Biggin et al²⁸ concluded that the variability of VGP dispersion curves may be reduced in times of increased dynamo stability. This finding may be extremely relevant to the present study. The coherence of the 2.45-2.82 Ga VGP dispersion curve is strikingly high given the noise we might expect to be introduced from the age of the rocks and the large amount of time that they are spanning. We speculate that this may be because the entire period of this time was characterised a pattern of PSV that was much less variable than that for the period 0-195 Myr.

Supplementary Information References

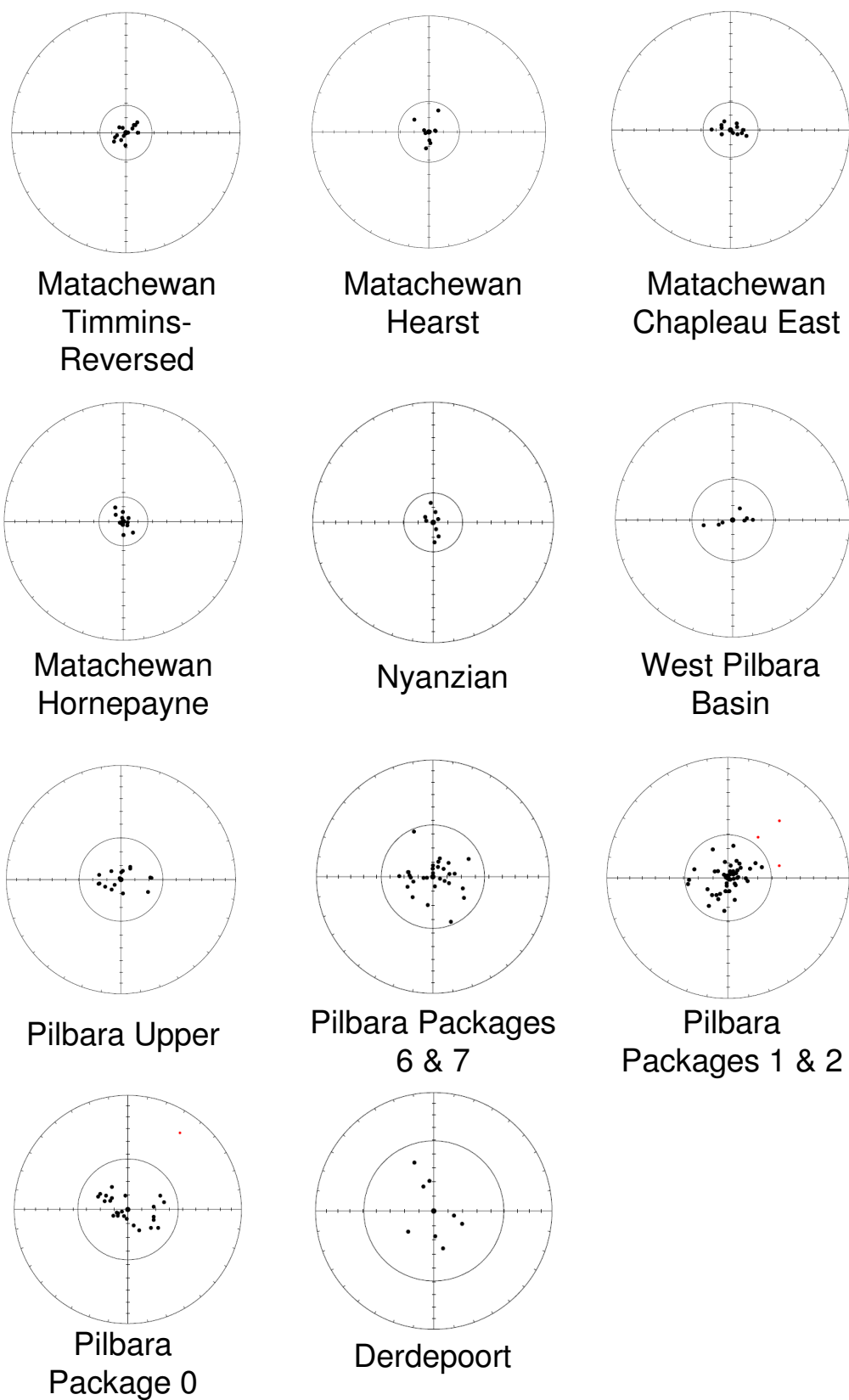
1. Strik, G. H. M. A., Blake, T. S., Zegers, T. E., White, S. H. & Langereis, C. G. Palaeomagnetism of flood basalts in the Pilbara Craton, Western Australia: Late Archaean continental drift and the oldest known reversal of the geomagnetic field. *Journal of Geophysical Research-Solid Earth* **108**, EPM 2-1 - EPM 2-21 (2003).
2. Strik, G. & Langereis, C. G. Palaeomagnetism of the late Archaean Nullagine and Mount Jope Supersequences, Western Australia. (in prep).
3. Strik, G. H. M. A. *Palaeomagnetism of late Archaean flood basalt terrains: implications for early Earth geodynamics and geomagnetism. Geologica Ultraiectina* (Utrecht, 2004).
4. Zijdeveld, J. D. A. in *Methods in palaeomagnetism* (ed. Runcorn, S. K.) 254-286 (Elsevier, New York, 1967).

5. Kirschvink, J. L. The least-squares line and plane and the analysis of palaeomagnetic data. *Geophys. J. R. Astron. Soc.* **62**, 699-718 (1980).
6. McFadden, P. L. & McElhinny, M. W. Classification of the Reversal Test in Paleomagnetism. *Geophysical Journal International* **103**, 725-729 (1990).
7. Creer, K. M. An analysis of the geomagnetic field using palaeomagnetic methods. *Journal of Geomagnetism and Geoelectricity* **13**, 113-119 (1962).
8. McElhinny, M. W. & McFadden, P. L. Palaeosecular variation over the past 5 Myr based on a new generalized database. *Geophysical Journal International* **131**, 240-252 (1997).
9. Creer, K. M. The dispersion of the geomagnetic field due to secular variation and its determination for remote times from palaeomagnetic data. *Journal of Geophysical Research* **67**, 3461-3476 (1962).
10. Cox, A. Analysis of present geomagnetic field for comparison with palaeomagnetic results. *Journal of Geomagnetism and Geoelectricity* **13**, 101-112 (1962).
11. Vandamme, D. A New Method to Determine Paleosecular Variation. *Physics of the Earth and Planetary Interiors* **85**, 131-142 (1994).
12. McElhinny, M. W., McFadden, P. L. & Merrill, R. T. The myth of the Pacific dipole window. *Earth and Planetary Science Letters* **143**, 13-22 (1996).
13. McFadden, P. L. & Jones, F. J. The discrimination of mean directions drawn from Fisher distributions. *Geophysical Journal of the Royal Astronomical Society* **67**, 19-33 (1981).
14. Bates, M. P. & Halls, H. C. Broad-Scale Proterozoic Deformation of the Central Superior-Province Revealed by Paleomagnetism of the 2.45 Ga Matachewan Dyke Swarm. *Canadian Journal of Earth Sciences* **28**, 1780-1796 (1991).
15. Halls, H. C. & Palmer, H. C. The tectonic relationship of two Early Proterozoic dyke swarms to the Kapuskasing Structural Zone: a paleomagnetic and petrographic study. *Canadian Journal of Earth Sciences* **27**, 87-103 (1990).
16. Halls, H. C. & Zhang, B. X. Uplift structure of the southern Kapuskasing zone from 2.45 Ga dike swarm displacement. *Geology* **26**, 67-70 (1998).
17. Halls, H. C. & Zhang, B. X. Crustal uplift in the southern Superior Province, Canada, revealed by paleomagnetism. *Tectonophysics* **362**, 123-136 (2003).
18. Delaney, P. T. Fortran-77 Programs for Conductive Cooling of Dikes with Temperature-Dependent Thermal-Properties and Heat of Crystallization. *Computers & Geosciences* **14**, 181-212 (1988).
19. Meert, J. G., VanderVoo, R. & Patel, J. Paleomagnetism of the Late Archean Nyanzian System, Western Kenya. *Precambrian Research* **69**, 113-131 (1994).
20. Many, S. & Maboko, M. A. H. Dating basaltic volcanism in the Neoproterozoic Sukumaland Greenstone Belt of the Tanzania Craton using the Sm-Nd method: implications for the geological evolution of the Tanzania Craton. *Precambrian Research* **121**, 35-45 (2003).
21. Blake, T. S., Buick, R., Brown, S. J. A. & Barley, M. E. Geochronology of a Late Archean flood basalt province in the Pilbara Craton, Australia: constraints on basin evolution, volcanic and sedimentary accumulation, and continental drift rates. *Precambrian Research* **133**, 143-173 (2004).

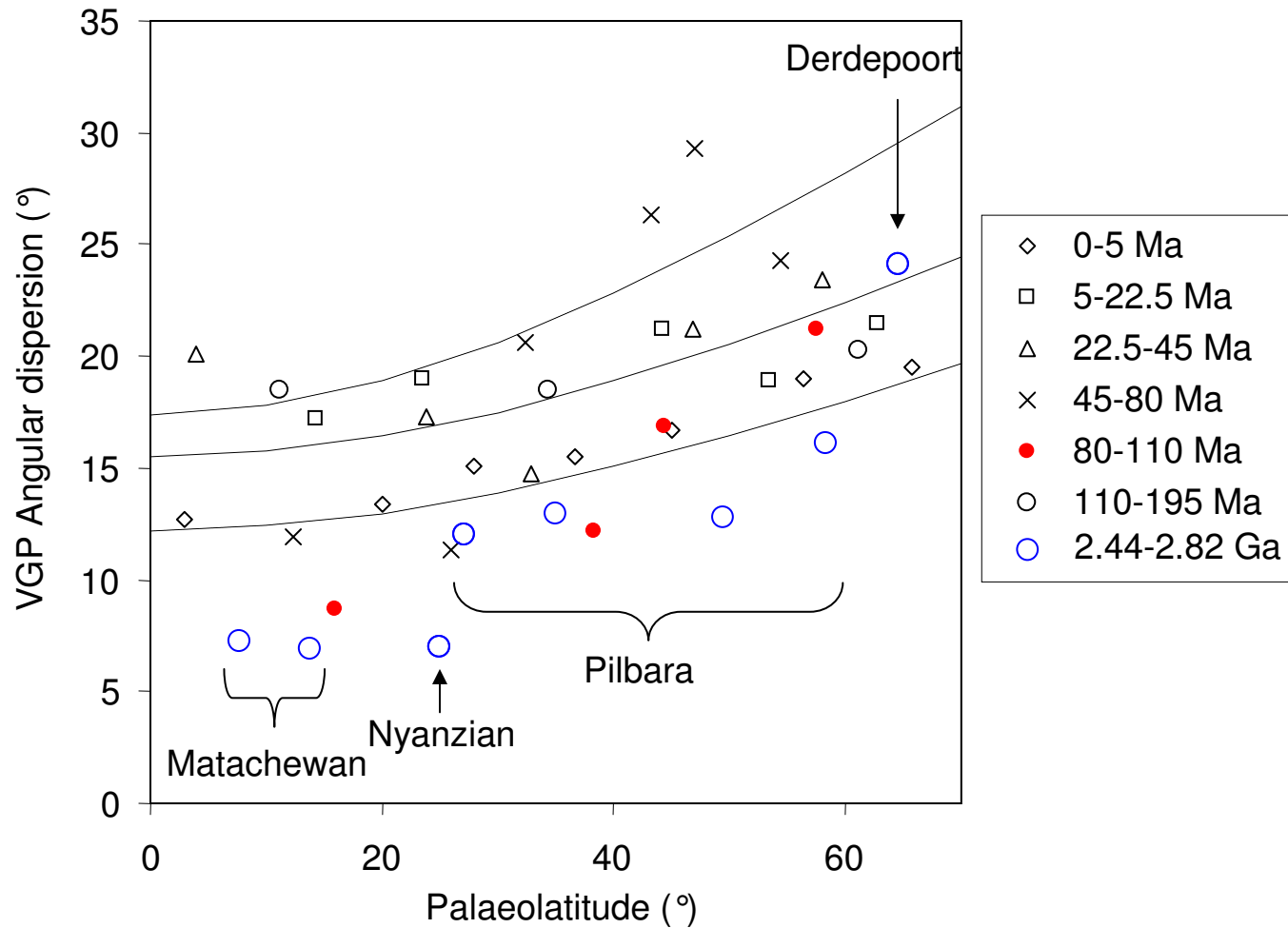
22. Wingate, M. T. D. A palaeomagnetic test of the Kaapvaal-Pilbara (Vaalbara) connection at 2.78 Ga. *South African Journal of Geology* **101**, 257-274 (1998).
23. Smirnov, A. V. & Tarduno, J. A. Secular variation of the Late Archean Early Proterozoic geodynamo. *Geophysical Research Letters* **31**, 10.1029/2004GL020333 (2004).
24. Mertanen, S., Halls, H. C., Vuollo, J. I., Pesonen, L. J. & Stepanov, V. S. Paleomagnetism of 2.44 Ga mafic dykes in Russian Karelia, eastern Fennoscandian Shield - implications for continental reconstructions. *Precambrian Research* **98**, 197-221 (1999).
25. McFadden, P. L., Merrill, R. T., McElhinny, M. W. & Lee, S. H. Reversals of the Earths Magnetic-Field and Temporal Variations of the Dynamo Families. *Journal of Geophysical Research-Solid Earth and Planets* **96**, 3923-3933 (1991).
26. Johnson, C. L. et al. Recent Investigations of the 0–5 Ma Geomagnetic Field Recorded by Lava Flows. *Geochemistry Geophysics Geosystems*, doi: 10.1029/2007GC001696, in press. (2008).
27. Tarduno, J. A., Cottrell, R. D. & Smirnov, A. V. The Cretaceous superchron geodynamo: Observations near the tangent cylinder. *Proceedings of the National Academy of Sciences of the United States of America* **99**, 14020-14025 (2002).
28. Biggin, A. J., van Hinsbergen, D., Langereis, C. G., Deenen, M. H. L. & Halden, M. M. Geomagnetic Secular variation in the Cretaceous Normal Superchron and in the Jurassic. *Physics of the Earth and Planetary Interiors*, Submitted (2008).



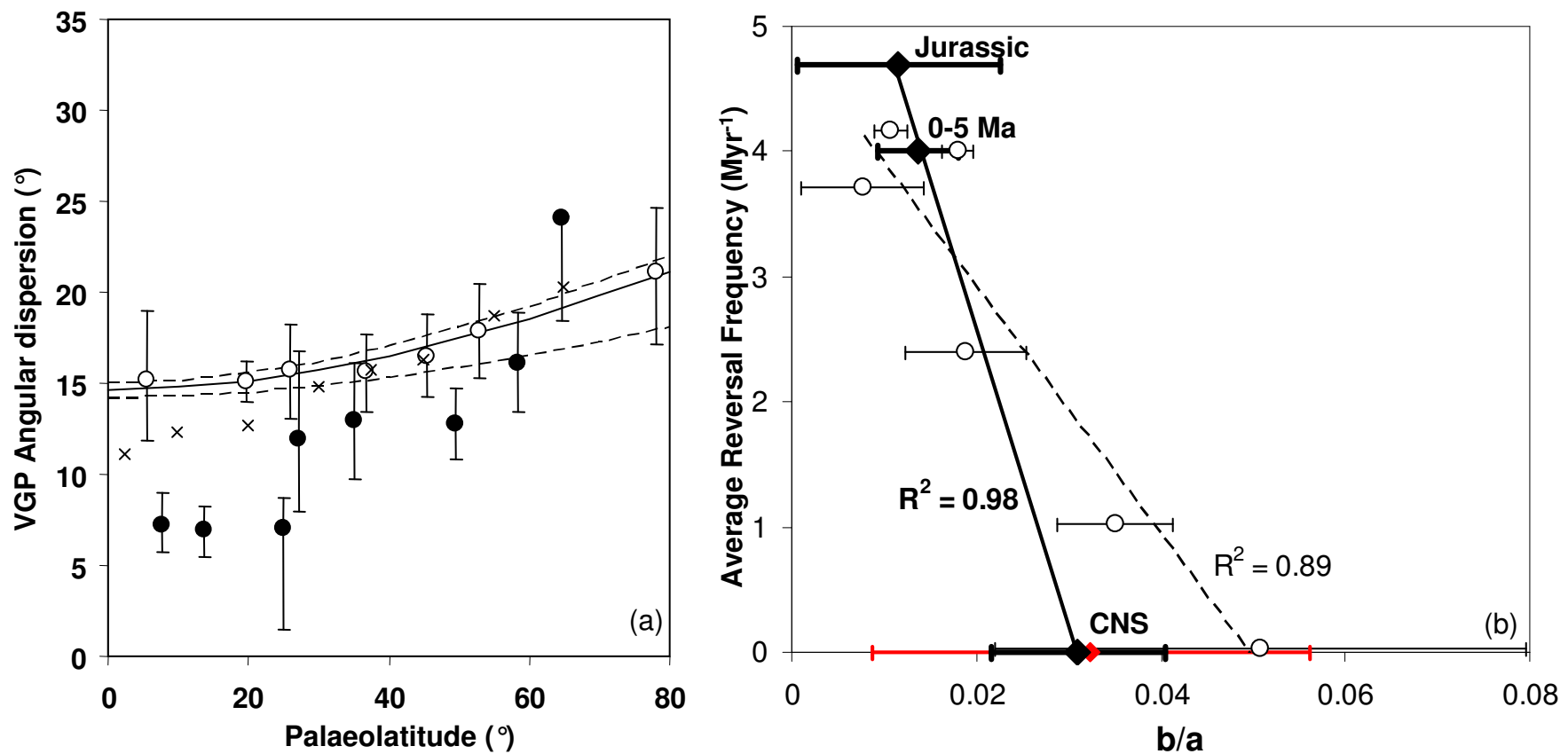
Supplementary figure 1: Examples of typical Zijderveld plots from each package of igneous units from the Pilbara Craton (including some plots which were rejected). Key temperatures (in °C) and field steps are shown.



Supplementary figure 2: Equal area plots of the VGPs of the datasets used in this study (c.f. table 1) with the mean VGP moved to the vertical. The circle represents the variable cutoff¹¹ (given in table 1) with excluded poles outside of the cutoff shown in red.



Supplementary Figure 3: A comparison of VGP dispersion curves from sub-periods within the period 0-195 Ma and for the period 2.44-2.82 Ga. The line shows the Model G fitted to the 0-195 Ma data (weighted by the corresponding length of time – see Methods) with its 95% bootstrap limits. The 2.44-2.82 Ga data are labelled with their sources.



Supplementary Figure 4: Comparisons of our data with recent studies of PSV in the period 0-200 Ma. (a) VGP dispersion plot showing hemispherically-combined and binned data from lavas from the period 0-5 Ma compiled by Johnson et al²⁶ (empty circles) together with Model G fit to them ($a = 14.7 +0.3 -0.5$, $b = 0.19 +0.01 -0.05$). Also shown are our 2.44-2,82 Ga data (filled circles) and the McElhinny et al⁸ data for the last 5 Myr (crosses). (b) The same plot as figure 2 in the main text with new data (filled diamonds) from 0-5 Ma²⁶, the Jurassic²⁷, and the Cretaceous Normal Superchron²⁷ shown. A linear regression through these data is shown. The original McFadden et al data²⁵ are shown as empty circles together with a regression line (dashed). The results of a more recent analysis of PSV in the CNS²⁸ is also shown as a red diamond. This and the CNS point of McFadden et al have large error bars because, in both cases, the Model G curve was fit to only four estimates of VGP dispersion.

| Area | PSVset | Package | Site Number | Lithology | AMG Coords (AGD 84) | Strike | Dip | N | n | dec° | inc° | k | a95° | R | Plat° | VGP lat° | VGP long° |
|------|-------------|---------|-------------|---------------|----------------------|--------|-----|----|----|-------|-------|--------|------|--------|-------|----------|-----------|
| MBB | Package 0 | 0 | GSP03 | Basalt | 50K 749404 - 7643594 | 055 | 46 | 9 | 8 | 299.7 | 69.1 | 116.1 | 5.2 | 7.94 | 52.6 | -0.5 | 87.6 |
| MBB | Package 0 | 0 | GSP04 | Basalt | 50K 749404 - 7643594 | 055 | 46 | 6 | 3 | 267.8 | 66.8 | 132.7 | 10.7 | 2.985 | 49.4 | -17.4 | 76.4 |
| MBB | Package 0 | 0 | GSP05 | Basalt | 50K 749404 - 7643594 | 055 | 46 | 7 | 3 | 304.6 | 67.8 | 57 | 16.5 | 2.965 | 50.8 | 3.1 | 88 |
| MBB | Package 0 | 0 | GSP06 | Basalt | 50K 749404 - 7643594 | 055 | 46 | 7 | 5 | 279.5 | 70.5 | 244 | 4.9 | 4.984 | 54.7 | -12 | 83.8 |
| MBB | Package 0 | 0 | GSP07 | Basalt | 50K 749404 - 7643594 | 055 | 46 | 6 | 5 | 295.7 | 67.2 | 270 | 4.7 | 4.985 | 49.9 | -1 | 84 |
| MBB | Package 0 | 0 | GSP08 | Basalt | 50K 749688 - 7644249 | 265 | 74 | 7 | 3 | 269.4 | 65.1 | 180.8 | 9.2 | 2.989 | 47.1 | -15.8 | 74.4 |
| MBB | Package 0 | 0 | GSP09 | Basalt | 50K 749688 - 7644249 | 265 | 74 | 7 | 5 | 267.1 | 73.2 | 116.4 | 7.1 | 4.966 | 58.9 | -19.6 | 86.2 |
| MBB | Package 0 | 0 | GSP10 | Basalt | 50K 749688 - 7644249 | 265 | 74 | 9 | 5 | 281 | 69 | 138.9 | 6.5 | 4.971 | 52.5 | -10.4 | 82 |
| MBB | Package 0 | 0 | GSP11 | Basalt | 50K 749688 - 7644249 | 265 | 74 | 7 | 4 | 273 | 68.8 | 516.3 | 4 | 3.994 | 52.2 | -14.9 | 80.1 |
| MBB | Package 0 | 0 | GSP12 | Basalt | 50K 749688 - 7644249 | 265 | 74 | 9 | 7 | 277.3 | 66.6 | 120 | 5.5 | 6.95 | 49.1 | -11.4 | 77.9 |
| MBB | Package 0 | 0 | GSP13 | Basalt | 50K 749688 - 7644249 | 265 | 74 | 5 | 3 | 289.4 | 75.7 | 66.6 | 15.2 | 2.97 | 63.0 | -10.5 | 93.6 |
| MBB | Package 0 | 0 | GSP14B* | Hyaloclastite | 50K 768095 - 7686388 | 113 | 36 | 8 | 8 | 185.4 | 78.1 | 5.7 | 25.3 | 6.779 | 67.1 | -43.6 | 116.7 |
| MBB | Package 0 | 0 | GSP16 | Basalt | 50K 770822 - 7637462 | 260 | 23 | 10 | 4 | 318.7 | 65.7 | 55.1 | 12.5 | 3.946 | 47.9 | 11.5 | 92.8 |
| MBB | Package 0 | 0 | GSP18A | Basalt | 50K 770852 - 7637517 | 260 | 23 | 8 | 6 | 308.6 | 67.2 | 88.9 | 7.1 | 5.944 | 49.9 | 5.5 | 89.3 |
| MBB | Package 0 | 0 | GSP18B* | Basalt | 50K 770852 - 7637517 | 260 | 23 | 7 | 3 | 291.3 | 51.8 | 10.3 | 40.5 | 2.806 | 32.4 | 5.2 | 67.5 |
| MBB | Package 0 | 0 | GSP19 | Basalt | 50K 770852 - 7637517 | 260 | 23 | 7 | 4 | 297.6 | 67.2 | 187.2 | 6.7 | 3.984 | 49.9 | 0 | 84.8 |
| MBB | Package 0 | 0 | GSP20 | Basalt | 50K 770852 - 7637517 | 260 | 23 | 7 | 6 | 295 | 64.6 | 233.8 | 4.4 | 5.979 | 46.5 | 0.4 | 81 |
| MBB | Package 0 | 0 | GSP21 | Basalt | 50K 770852 - 7637517 | 260 | 23 | 7 | 7 | 298.5 | 66.1 | 334.2 | 3.3 | 6.982 | 48.5 | 1.3 | 83.9 |
| MBB | Package 0 | 0 | GSP81 | Basalt | 50K 762058 - 7687748 | 035 | 44 | 7 | 7 | 339.6 | 71.8 | 274.4 | 3.7 | 6.978 | 56.7 | 10.6 | 108.3 |
| MBB | Package 0 | 0 | GSP82 | Basalt | 50K 762063 - 7687732 | 035 | 44 | 7 | 5 | 353.9 | 80.2 | 96.2 | 7.8 | 4.958 | 70.9 | -1.9 | 117.5 |
| MBB | Package 0 | 0 | GSP83 | Basalt | 50K 762343 - 7687328 | 035 | 44 | 7 | 6 | 357.6 | 77.5 | 173.8 | 5.1 | 5.971 | 66.1 | 3 | 118.5 |
| MBB | Package 0 | 0 | GSP84 | Basalt | 50K 762347 - 7687315 | 035 | 44 | 7 | 4 | 340 | 70.3 | 273.2 | 5.6 | 3.989 | 54.4 | 12.8 | 107.7 |
| MBB | Package 0 | 0 | GSP85 | Basalt | 50K 762426 - 7687252 | 035 | 44 | 7 | 7 | 337.3 | 66.3 | 159.8 | 4.8 | 6.962 | 48.7 | 17.5 | 104 |
| MBB | Package 0 | 0 | GSP86 | Basalt | 50K 762461 - 7687281 | 035 | 44 | 7 | 6 | 345.3 | 66.3 | 512.5 | 3 | 5.99 | 48.7 | 19.2 | 109.3 |
| MBB | Package 0 | 0 | GSP87 | Basalt | 50K 762368 - 7686443 | 035 | 44 | 7 | 4 | 119.9 | 69.7 | 38 | 15.1 | 3.921 | 53.5 | -34.3 | 158.1 |
| MBB | Package 0 | 0 | GSP88* | Basalt | 50K 762392 - 7686373 | 035 | 44 | 8 | 5 | 189.5 | 83 | 15.1 | 20.3 | 4.736 | 76.2 | -34.5 | 116.8 |
| MBB | Package 0 | 0 | GSP89 | Basalt | 50K 765454 - 7686832 | 070 | 28 | 8 | 8 | 339.1 | 76.1 | 125.4 | 5 | 7.994 | 63.7 | 3.9 | 110.4 |
| MBB | Package 0 | 0 | GSP90 | Basalt | 50K 765529 - 7686812 | 070 | 28 | 7 | 6 | 325.5 | 63.9 | 56.9 | 9 | 5.912 | 45.6 | 16.5 | 95.1 |
| WPB | Lower Group | 1 | GSP125 | Basalt | 50K 511632 - 7686995 | 320 | 20 | 7 | 4 | 117.3 | 57.3 | 163.1 | 7.1 | 3.982 | 37.9 | -33.9 | 174.7 |
| WPB | Lower Group | 1 | GSP126 | Basalt | 50K 511651 - 7686984 | 320 | 20 | 8 | 7 | 90.3 | 60.9 | 437.7 | 2.9 | 6.986 | 41.9 | -14.0 | 167.2 |
| WPB | Lower Group | 1 | GSP127 | Basalt | 50K 511623 - 7685943 | 320 | 20 | 7 | 5 | 90 | 67.1 | 35.2 | 13.1 | 4.886 | 49.8 | -15.8 | 159.2 |
| WPB | Lower Group | 1 | GSP128 | Basalt | 50K 511741 - 7685642 | 320 | 20 | 9 | 8 | 113.6 | 56.9 | 52.9 | 7.7 | 7.868 | 37.5 | -30.9 | 175.1 |
| WPB | Lower Group | 1 | GSP129 | Basalt | 50K 511865 - 7685658 | 320 | 20 | 7 | 4 | 135.9 | 69.4 | 24.2 | 19.1 | 3.876 | 53.1 | -43.5 | 152.3 |
| WPB | Lower Group | 1 | GSP130 | Basalt | 50K 511614 - 7685457 | 320 | 20 | 8 | 4 | 115 | 70.1 | 51.8 | 12.9 | 3.942 | 54.1 | -31.4 | 155.6 |
| WPB | Lower Group | 1 | GSP131 | Basalt | 50K 512567 - 7686094 | 320 | 20 | 8 | 7 | 271 | -58.4 | 34.4 | 10.4 | 6.825 | 39.1 | 13.8 | 350.1 |
| MBB | Lower Group | 1 | GSP147 | Basalt | 50K 781652 - 7652819 | 111 | 15 | 7 | 5 | 132.8 | 66.8 | 113.9 | 7.2 | 4.965 | 49.4 | -43.4 | 160.8 |
| MBB | Lower Group | 1 | GSP148 | Basalt | 50K 781660 - 7652857 | 111 | 15 | 7 | 5 | 137.6 | 67.5 | 61.5 | 9.8 | 4.935 | 50.4 | -45.9 | 157.9 |
| MBB | Lower Group | 1 | GSP149 | Basalt | 50K 781665 - 7652903 | 111 | 15 | 8 | 8 | 125.6 | 64.6 | 218.2 | 3.8 | 7.968 | 46.5 | -39.5 | 166.2 |
| MBB | Lower Group | 1 | GSP150 | Basalt | 50K 781658 - 7652955 | 111 | 15 | 7 | 5 | 146.3 | 64.6 | 1300.8 | 2.1 | 4.997 | 46.5 | -52.8 | 158.9 |
| MBB | Lower Group | 1 | GSP162 | Basalt | 50K 781775 - 7652781 | 111 | 15 | 7 | 6 | 145.1 | 66.2 | 381.7 | 3.4 | 5.987 | 48.6 | -51 | 156.7 |
| MBB | Lower Group | 1 | GSP163 | Basalt | 50K 781720 - 7652790 | 111 | 15 | 7 | 7 | 132.7 | 69 | 188.1 | 4.4 | 6.968 | 52.5 | -42.2 | 156.9 |
| MBB | Lower Group | 1 | GSP164 | Basalt | 50K 781696 - 7652810 | 111 | 15 | 7 | 7 | 133.5 | 64.3 | 105.4 | 5.9 | 6.943 | 46.1 | -44.9 | 164.9 |
| NOS | Lower Group | 1 | GSP174 | Basalt | 51K 218927 - 7675571 | 306 | 15 | 7 | 5 | 141.7 | 73.4 | 231.1 | 5 | 4.983 | 59.2 | -43.1 | 146.1 |
| NOS | Lower Group | 1 | GSP175 | Basalt | 51K 219018 - 7675625 | 306 | 15 | 7 | 4 | 161 | 71.4 | 167.9 | 7.1 | 3.982 | 56.1 | -52.2 | 137.6 |
| NOS | Lower Group | 1 | GSP176 | Basalt | 51K 219181 - 7675678 | 306 | 15 | 15 | 11 | 134.3 | 63.5 | 54.8 | 6.2 | 10.817 | 45.1 | -45.6 | 166.5 |
| NOS | Lower Group | 1 | GSP177 | Basalt | 51K 219353 - 7675765 | 326 | 21 | 7 | 3 | 122.2 | 74.4 | 597.4 | 5 | 2.997 | 60.8 | -33.7 | 150 |
| NG | Lower Group | 1 | GSP190 | Basalt | 50K 596927 - 7621919 | 010 | 10 | 8 | 5 | 119.2 | 54.8 | 41.4 | 12 | 4.903 | 35.3 | -35.6 | 179.1 |
| NG | Lower Group | 1 | GSP196 | Basalt | 50K 597712 - 7622787 | 010 | 10 | 7 | 7 | 189.2 | 78.7 | 594.6 | 2.5 | 6.99 | 68.2 | -42.9 | 113.3 |
| NG | Lower Group | 1 | GSP197 | Basalt | 50K 597687 - 7622875 | 010 | 10 | 7 | 5 | 181.2 | 64 | 16.6 | 19.3 | 4.759 | 45.7 | -65.8 | 115.9 |
| MBB | Lower Group | 1 | GSP24 | Basalt | 50K 770457 - 7639104 | 258 | 17 | 7 | 7 | 99.2 | 78.1 | 267.8 | 3.7 | 6.978 | 67.1 | -23.1 | 144.2 |
| MBB | Lower Group | 1 | GSP25 | Basalt | 50K 767635 - 7643347 | 332 | 14 | 11 | 8 | 111.6 | 69.7 | 243.3 | 3.6 | 7.971 | 53.5 | -29.7 | 159.1 |
| MBB | Lower Group | 1 | GSP26 | Basalt | 50K 767429 - 7643505 | 332 | 14 | 9 | 9 | 124.5 | 67.6 | 212 | 3.5 | 8.962 | 50.5 | -38 | 161.3 |
| MBB | Lower Group | 1 | GSP27 | Basalt | 50K 767429 - 7643505 | 332 | 14 | 8 | 8 | 122.4 | 68.8 | 718.5 | 2.1 | 7.99 | 52.2 | -36.4 | 159.6 |
| MBB | Lower Group | 1 | GSP28 | Basalt | 50K 767286 - 7643426 | 332 | 14 | 7 | 7 | 132.5 | 69.8 | 144.8 | 5 | 6.959 | 53.7 | -41.7 | 155.4 |
| MBB | Lower Group | 1 | GSP29 | Basalt | 50K 767286 - 7643426 | 332 | 14 | 7 | 5 | 126 | 68.5 | 1144.7 | 2.3 | 4.997 | 51.8 | -38.6 | 159.4 |
| MBB | Lower Group | 1 | GSP30 | Basalt | 50K 767286 - 7643426 | 332 | 14 | 6 | 6 | 129.4 | 69.2 | 191.3 | 4.9 | 5.974 | 52.8 | -40.3 | 157.4 |

| | | | | | | | | | | | | | | | | | |
|-----|--------------------|----|---------|-------------------------|----------------------|-----------|----|----|----|-------|-------|-------|------|--------|------|-------|-------|
| MBB | Lower Group | 1 | GSP31 | Basalt | 50K 767143 - 7643347 | 332 | 14 | 7 | 7 | 127.9 | 66.5 | 453 | 2.8 | 6.987 | 49.0 | -40.5 | 162.5 |
| MBB | Lower Group | 1 | GSP32 | Basalt | 50K 767143 - 7643347 | 332 | 14 | 7 | 7 | 128.3 | 60.3 | 144.5 | 5 | 6.958 | 41.2 | -42.3 | 172.6 |
| NOS | Lower Group | 2 | GSP179 | Massive dacite porphyry | 51K 219910 - 7676547 | 312 | 25 | 7 | 5 | 317 | -80.6 | 52.1 | 10.7 | 4.923 | 71.7 | 33.7 | 315.2 |
| NOS | Lower Group | 2 | GSP181 | Massive dacite porphyry | 51K 216455 - 7679722 | 304 | 15 | 7 | 6 | 345.3 | -68.5 | 80.4 | 7.5 | 5.938 | 51.8 | 57.1 | 317.1 |
| BCA | Lower Group | 6 | GSP43 | Basalt | 51K 274691 - 7597559 | Sub-Horiz | | 7 | 3 | 143 | 61.6 | 41.6 | 19.4 | 2.952 | 42.8 | -52.7 | 167.7 |
| WPB | Lower Group | 7 | GSP100 | Basalt | 50K 500550 - 7646454 | Sub-Horiz | | 7 | 7 | 164.9 | 70 | 105.4 | 5.9 | 6.943 | 53.9 | -55.4 | 132.7 |
| WPB | Lower Group | 7 | GSP105 | Basalt | 50K 495805 - 7645380 | Sub-Horiz | | 10 | 8 | 195.5 | 47.9 | 449.2 | 2.6 | 7.984 | 29.0 | -74.0 | 58.8 |
| WPB | | 7 | GSP117 | mafic sill | 50K 510344 - 7679863 | Sub-Horiz | | 8 | 5 | 320.6 | -68.4 | 86.3 | 8.3 | 4.954 | 51.6 | 46.8 | 332.2 |
| WPB | | 7 | GSP118 | mafic sill | 50K 508878 - 7677632 | Sub-Horiz | | 13 | 10 | 346.7 | -65.8 | 70.3 | 5.8 | 9.872 | 48.0 | 60.9 | 315.5 |
| WPB | | 7 | GSP119 | mafic sill | 50K 511788 - 7673204 | | 02 | 6 | 6 | 175.6 | 64.7 | 81.8 | 7.5 | 5.939 | 46.6 | -64.2 | 124.1 |
| WPB | | 7 | GSP120 | mafic sill | 50K 512041 - 7673398 | | 02 | 7 | 7 | 166.8 | 72.4 | 131.4 | 5.3 | 6.954 | 57.6 | -52.2 | 128.6 |
| WPB | Lower Group | 7 | GSP132 | Basalt | 50K 495995 - 7646990 | | 06 | 13 | 6 | 148.7 | 68.7 | 100.7 | 6.7 | 5.95 | 52.1 | -50.9 | 147.4 |
| WPB | Lower Group | 7 | GSP205 | Basalt | 50K 506601 - 7645979 | 086 | 06 | 7 | 5 | 162.1 | 68.9 | 123.4 | 6.9 | 4.986 | 52.3 | -56.0 | 136.7 |
| WPB | Lower Group | 7 | GSP206 | Basalt | 50K 507398 - 7645186 | 086 | 06 | 7 | 7 | 149.8 | 58.1 | 58.1 | 8 | 6.897 | 38.8 | -58.8 | 166.2 |
| WPB | Lower Group | 7 | GSP207 | Basalt | 50K 506962 - 7643331 | 086 | 06 | 7 | 3 | 149.4 | 38.3 | 62.2 | 15.8 | 2.968 | 21.5 | -61.6 | 200.9 |
| BCA | Lower Group | 7 | GSP47 | Basalt | 51K 278215 - 7601882 | Sub-Horiz | | 10 | 3 | 157.1 | 79.1 | 146.4 | 10.2 | 2.986 | 68.9 | -40.7 | 131.5 |
| BCA | Lower Group | 7 | GSP48 | Mafic tuff | 51K 278052 - 7601808 | Sub-Horiz | | 10 | 3 | 165.4 | 55.5 | 172.1 | 9.4 | 2.988 | 36.0 | -70.8 | 159.2 |
| BCA | Lower Group | 7 | GSP49 | Basalt | 51K 279149 - 7603472 | Sub-Horiz | | 10 | 8 | 327.2 | -62.9 | 39.2 | 9 | 7.821 | 44.3 | 54.8 | 343 |
| WPB | West Pilbara Basin | 8 | GSP108 | Basalt | 50K 492325 - 7640458 | 319 | 11 | 7 | 5 | 139.5 | 44.9 | 137.9 | 6.5 | 4.971 | 26.5 | -52.8 | 190.8 |
| WPB | West Pilbara Basin | 8 | GSP109 | Basalt | 50K 492380 - 7640500 | 319 | 11 | 3 | 3 | 146.2 | 44.9 | 180 | 9.2 | 2.989 | 26.5 | -58.8 | 190.7 |
| WPB | West Pilbara Basin | 8 | GSP110 | Basalt | 50K 492418 - 7640563 | 319 | 11 | 8 | 5 | 141.6 | 46.8 | 25.5 | 15.4 | 4.843 | 28.0 | -54.6 | 188.2 |
| WPB | West Pilbara Basin | 8 | GSP111 | Basalt | 50K 492461 - 7640589 | 319 | 11 | 5 | 4 | 122.6 | 43.3 | 97.2 | 9.4 | 3.969 | 25.2 | -37.5 | 190.9 |
| WPB | West Pilbara Basin | 8 | GSP112 | Basalt | 50K 492464 - 7640592 | 319 | 11 | 5 | 4 | 108.6 | 38.8 | 156.4 | 7.4 | 3.981 | 21.9 | -24.3 | 191.7 |
| WPB | West Pilbara Basin | 8 | GSP199 | Basalt | 50K 507371 - 7642673 | 86 | 06 | 7 | 4 | 119.8 | 41.1 | 78.8 | 10.4 | 3.962 | 23.6 | -34.7 | 192.5 |
| BCA | Upper | 8 | GSP58 | Basalt | 51K 281732 - 7611993 | Sub-Horiz | | 7 | 4 | 181.4 | 42.4 | 25.3 | 18.6 | 3.882 | 24.5 | -86.8 | 97.6 |
| NOS | Upper | 9 | GSP185 | Basalt | 51K 250351 - 7675774 | 066 | 16 | 8 | 3 | 186.6 | 53 | 90.5 | 13 | 2.978 | 33.6 | -76.1 | 97 |
| NOS | Upper | 9 | GSP186 | Basalt | 51K 250317 - 7675850 | 062 | 16 | 7 | 5 | 140.5 | 56.6 | 66.6 | 9.4 | 4.94 | 37.2 | -52.2 | 176.5 |
| WPB | West Pilbara Basin | 10 | GSP140 | Basalt | 50K 479857 - 7625447 | 315 | 08 | 7 | 5 | 136.5 | 54.6 | 76.6 | 8.8 | 4.948 | 35.1 | -49.7 | 177.3 |
| WPB | | 10 | GSP142* | Basalt | 50K 480974 - 7625127 | 315 | 08 | 7 | 3 | 164.7 | 75.1 | 33.6 | 21.6 | 2.941 | 62.0 | -48.2 | 127.5 |
| NOS | Upper | 10 | GSP69A | Basalt | 51K 244972 - 7666272 | 295 | 03 | 7 | 7 | 169.4 | 62.7 | 597.1 | 2.5 | 6.99 | 44.1 | -65.4 | 139.0 |
| NOS | Upper | 10 | GSP69B | Basalt | 51K 244902 - 7666287 | 295 | 03 | 7 | 7 | 169.2 | 61.7 | 677.2 | 2.3 | 6.991 | 42.9 | -66.4 | 140.6 |
| NOS | Upper | 10 | GSP70 | Basalt | 51K 241713 - 7671205 | 290 | 02 | 12 | 12 | 160.5 | 59.7 | 388.8 | 2.2 | 11.972 | 40.6 | -64.4 | 156.5 |
| NOS | Upper | 10 | GSP71 | Basalt | 51K 242817 - 7670512 | 290 | 02 | 10 | 10 | 162 | 60.6 | 46.5 | 7.2 | 9.806 | 41.6 | -64.5 | 153.0 |
| NOS | Upper | 10 | GSP72 | Basalt | 51K 240916 - 7668901 | 290 | 02 | 10 | 10 | 151 | 60.2 | 98.9 | 4.9 | 9.909 | 41.1 | -58.3 | 164.6 |
| WPB | | 11 | GSP143 | Basalt | 50K 479675 - 7615872 | 315 | 08 | 9 | 9 | 137.4 | 77.7 | 75.4 | 6 | 8.894 | 66.4 | -37.6 | 136.8 |
| WPB | | 11 | GSP144* | Basalt | 50K 479982 - 7615433 | 315 | 08 | 9 | 3 | 159.1 | 58.8 | 30.8 | 22.6 | 2.935 | 39.5 | -64.7 | 156.8 |

Supplementary Table 1: Summary of new HT results from the Pilbara Craton. AMG refers to Australia Map Grid

Areas: BCA is Boodalyerri Creek Area, MBB is Marble Bar basin, NOS is North Oakover Syncline, WPB is West Pilbara Basin.

Where sample codes are marked with *, the mean direction failed selection criteria ($n \geq 3$, $\alpha 95 < 20$) and is not used in the PSV analysis

Note that bedding plane strikes and dip follow the right-hand convention,